PNAS
www.pnas.org

Supplementary Information for

Fast oxidation of sulfur dioxide by hydrogen peroxide in deliquesced aerosol particles

Tengyu Liu,[*,1] *Simon L. Clegg,*[2] *and Jonathan P. D. Abbatt*[*,1]
[1] *Department of Chemistry, University of Toronto, Toronto, ON, M5S 3H6, Canada.*
[2] *School of Environmental Sciences, University of East Anglia, Norwich NR4 7TJ, U.K.*

Tengyu Liu and Jonathan P. D. Abbatt
Email: tengyu.liu@utoronto.ca, jonathan.abbatt@utoronto.ca

This PDF file includes:

Supplementary text
Figures S1 to S10
Tables S1 to S5
SI References

Supplementary Information Text

1 Flow tube experiments and instrument operation

1.1 Flow tube experiments

A schematic of the experimental setup is shown in Fig. S1. All experiments were conducted in a vertically oriented pyrex flow tube (length 95 cm, inner diameter 6.2 cm) at a total flow rate of 1500 sccm at laminar flow conditions (Re ~34). The interior walls of the flow tube were coated with a thin layer of halocarbon wax to minimize the wall loss of SO_2 and H_2O_2. A constant output atomizer (TSI Aerosol Generator 3076), operated at a flow rate of 3 slpm, was used to generate pH-buffered polydisperse deliquesced aerosol particles from the following solutions: A. a mixture of NaCl/malonic acid/sodium bimalonate (10/0.5/0.5 mM, 3/0.5/0.5 mM, and 1/0.5/0.5 mM), B. NaCl/sodium bimalonate/sodium malonate (10/0.5/0.5 mM, 3/0.5/0.5 mM, and 1/0.5/0.5 mM), C. $NaNO_3$/malonic acid/sodium bimalonate (10/0.5/0.5 mM), D. $NaNO_3$/sodium bimalonate/sodium malonate (10/0.5/0.5 mM), E. malonic acid/sodium bimalonate (5/5 mM), and F. sodium bimalonate/sodium malonate (5/5 mM). The solutions were freshly prepared before each experiment. A fraction of the humidified aerosol flow was passed through a Kr-85 neutralizer (TSI Inc.) and mixed with a humidified N_2 flow and a dry SO_2 flow and then entered the kinetics flow tube from the side inlet perpendicular to the flow tube. The majority of the atomizer output went to the exhaust. The humidified N_2 flow was produced by bubbling N_2 gas (from liquid N_2) through MilliQ water. SO_2 was delivered by a flow of 10, 25, or 50 sccm from a cylinder (11 ppm in N_2, Linde) to achieve three different SO_2 concentrations in the flow tube. Three different gas-phase H_2O_2 mixing ratios were achieved by bubbling 10 sccm N_2 gas through an aqueous H_2O_2 solution (15% by weight) and 20 sccm N_2 gas through a 15% or 30% H_2O_2 solution. The H_2O_2 flow was introduced into the central portion of the

58 humidified aerosol flow through a 3-mm O.D. PFA Teflon tube shielded with a 6-mm O.D.
59 movable stainless steel injector tube that is inserted axially down the center of the flow
60 tube, enabling variable reaction times. The flow was drawn down the flow tube by the
61 pumping action of a scanning mobility particle sizer (SMPS), an aerosol mass spectrometer
62 (AMS), an SO_2 monitor, and an additional pump. For supplementary experiments, an H_2O_2
63 monitor was connected instead of the pump to quantify the H_2O_2 concentrations in the
64 absence of seed aerosols. All experiments were carried out at 21-25 ºC and RH of 73-90%
65 (Table S1). RH was measured by an in-line digital hygrometer (Vaisala M170). The RH
66 was controlled by adjusting the humidity of the humidified N_2 flow and kept constant to
67 within ~1% over the course of an experiment. Note that all the H_2O_2/SO_2 experiments were
68 conducted in N_2 carrier gas to minimize the potential for O_2 oxidation of the SO_2.
69 For each kinetics run, the aerosol particles were first characterized in the presence of
70 SO_2 and the absence of H_2O_2 to quantify the background sulfate formation between the
71 interaction of SO_2 and seed aerosols. Then the aqueous oxidation of SO_2 was initiated by
72 introducing H_2O_2. The reaction time was adjusted by pushing the movable injector all the
73 way in the flow tube in a stepwise manner from 60 cm to 10 cm away from the bottom.
74 Reverse order of pulling the movable injector all the way out did not affect the sulfate
75 formation rate. Fig. S2 shows the time series of RH, SO_2, particle volume, organics and
76 sulfate concentrations for a typical experiment. As described above, the RH was stable over
77 the course of the experiment. The sulfate concentration decreased with the decrease of the
78 reaction time while the volumes of dry and wet aerosol particles remained relatively
79 invariable. For the quantification of sulfate, the background sulfate signal was subtracted
80 from the total steady-state sulfate concentrations. The contributions of background sulfate

to the total steady-state sulfate concentrations were all less than 7%. For aerosol particles with only organic buffer present, the estimated buffer capacity (defined as the amount of H^+ needed to change the pH by 1 unit) can buffer 2.5 – 4.3 molal of H^+, which is typically higher than the amount of H^+ formed. However, for the particles containing NaCl or $NaNO_3$, the estimated buffer capacity is 0.1 – 1.3 molal of H^+, which is lower than the amount of H^+ formed for some data points. It is possible that HCl or HNO_3 evaporate from the particles under those conditions, removing acidity.

1.2 Instrument operation

Compact and high-resolution time-of-flight aerosol mass spectrometers (1) (C-ToF-AMS and HR-ToF-AMS; Aerodyne Research) were deployed to characterize the concentration and chemical composition of aerosol particles for experiments with and without NaCl present, respectively. The HR-ToF-AMS was operated in the high sensitivity V-mode with a time resolution of 1 minute. The toolkit Squirrel 1.60Q and Pika 1.20Q were used to analyze the AMS data. The concentration of sulfate ($\mu g\ m^{-3}$) was calculated by summing the nitrate-equivalent masses of each high-resolution ion associated with the sulfate fraction. The sulfate was measured in the form of sodium sulfate since the sulfuric acid that forms was buffered by sodium bimalonate or sodium malonate. For sodium sulfate, there is no pathway to produce water fragments after vaporization and ionization. Therefore, a sulfate fragmentation table without water fragments was used (2). Prior to the experiments, the ionization efficiency (IE) of the AMS was calibrated using 300 nm ammonium nitrate particles. The relative ionization efficiency (RIE) of sulfate was determined for sodium sulfate. Polydisperse pure sodium sulfate was atomized to the AMS and SMPS simultaneously. The sodium sulfate particles were passed through a diffusion dryer to

104 remove aerosol water before they were sampled to the SMPS, while they were kept in the
105 liquid phase without passing through a diffusion dryer prior to characterization by AMS,
106 wherein the collection efficiency of particles was assumed to be unity (3). The particle size
107 distributions measured by SMPS were converted to mass concentrations using the density
108 of sodium sulfate of 2.68 g cm^{-3} (4), and converted to sulfate concentrations via the sulfate
109 mass fraction of sodium sulfate. The RIE of sulfate was derived by comparing the sulfate
110 concentrations measured by AMS and SMPS, determined to be 0.12 and 0.24 for C-ToF-
111 AMS and HR-ToF-AMS, respectively. The higher RIE for HR-ToF-AMS is likely due to
112 its higher vaporizer power of 5 Watt than that of 4.6 Watt for C-ToF-AMS. After applying
113 the RIE calibration, the difference between sulfate concentrations simultaneously
114 measured by these two AMS was within 10%.
115 The SMPS instrument consists of a differential mobility analyzer (DMA, TSI 3081)
116 and a condensation particle counter (CPC, TSI 3772). The aerosol and sheath flow rates
117 were 0.3 and 3 L min^{-1}, respectively, allowing for a size distribution scans ranging from
118 15–410 nm.
119 **1.3 Choice of aerosol systems**
120 The constraints for the experiment were to: i) work with aerosol components with variable
121 hygroscopicity, to enable variations in solute strength, ii) have the ability to add pH buffers
122 to the particles, iii) use aerosol particle solutions for which there are rigorous
123 thermodynamic predictions of hygroscopicity and acidity, and iv) have the ability for
124 sulfate yields to be accurately quantified with an aerosol mass spectrometer.
125 As a result, i) We chose to work with NaCl, $NaNO_3$, and organic acid particles, given
126 their variable hygroscopicities. ii) To control the pH, we chose to use organic acid buffers

given that the malonate/bimalonate/malonic acid system establishes pH values close to those of atmospheric aerosol. As well, organic acids are common urban aerosol constituents. iii) All of the individual components (chloride, sodium, nitrate malonate/bimalonate/malonic acid) are modelled by the E-AIM thermodynamic model, allowing for pH and ionic strength assessments. Note, for example, that we considered using phosphate pH buffers but they are not in E-AIM, nor are they atmospherically relevant. iv) These experiments cannot be conducted with an aerosol system largely composed of sulfate (e.g. $(NH_4)_2SO_4$) because sulfate is the reaction product, i.e. it is required to start with low sulfate mass loadings so that the formation of sulfate can be clearly observed during the reaction. Similarly, we could not use NH_4^+ as an initial component of the aerosol particles because the formation of $(NH_4)_2SO_4$ during the reaction would drastically change the sensitivity of the AMS to sulfate during the experiment (because the relative ionization efficiency of sulfate in $(NH_4)_2SO_4$ is very different from that of Na_2SO_4). In particular, as the reaction proceeded, a varying ratio of $(NH_4)_2SO_4$ to Na_2SO_4 would be formed. By only using Na^+ as the cation in the particles, we are fully confident that the reaction product is Na_2SO_4, which is a species for which the aerosol mass spectrometer can be calibrated. As well, by not using NH_4^+ as the cation, we avoid complications arising from NH_3 evaporation, with associated impacts on aerosol pH.

2 Modeled SO_4^{2-} formation rate

Modeled sulfate formation rates were calculated based on the literature parameters of aqueous SO_2 oxidation by H_2O_2 obtained in bulk solutions, without taking the effects of ionic strength and general acid catalysis into account. The rate expressions, rate coefficients and equilibrium constants that we used to calculate the aqueous-phase

150 concentrations of SO_2 and H_2O_2 are shown in Tables S2 and S3, respectively. Note that we
151 assume the sulfate formation rate in molal s^{-1} equals to that in M s^{-1} for the dilute solutions.
152 The modeled enhancement factors of sulfate formation rate in the main text Fig. 2C
153 were calculated based on parameters obtained in bulk solutions (5-7) for ionic strength of
154 0-5 molal, accounting for the overall effects of ionic strength on the proton-catalyzed
155 reaction rate coefficient *k*, Henry's law constants of H_2O_2 and SO_2, and the first
156 stoichiometric dissociation constant of H_2SO_3. The effects of ionic strength on the reaction
157 rate coefficient *k* and equilibrium constants are shown in Table S4 and Fig. S5. With the
158 increase of ionic strength, the reaction rate coefficient *k* decreases first, followed by a
159 minimum and then an increase while the first stoichiometric dissociation constant of H_2SO_3
160 shows a reverse trend. Increasing the ionic strengths, the Henry's law constants of H_2O_2
161 and SO_2 show trends of slight increase and decrease, respectively.
162 Also, we performed very preliminary calculations to assess how ionic strength in an
163 ammonium sulfate particle may affect reactant concentrations, as compared to the results
164 for NaCl and $NaNO_3$. The two Henry's law constants on the right hand side of Equation (1)
165 of the main paper both involve uncharged solution species. The sulfate ion tends to have a
166 salting-out effect relative to Na^+, Cl^- and NO_3^-, so it is expected that the stoichiometric
167 values of H_{SO2} and H_{H2O2} are somewhat smaller in a largely SO_4^{2-} medium. However, the
168 activity coefficients of such species generally vary less with the composition of the solution
169 than do those of ions, consequently the salt effects on the dissociation constant K_{a1}^* are
170 likely to be much larger. If it is assumed that the activity coefficients of H^+ and HSO_3^- have
171 approximately the same values in aqueous $(NH_4)_2SO_4$ as H^+ and HSO_4^-, we calculate that
172 the stoichiometric value of K_{a1}^* is increased by the following factors relative to its value in

NaCl: 21 (90% RH, I_{NaCl} = 2.8 mol kg^{-1}, $I_{(NH4)2SO4}$ = 9.2 mol kg^{-1}) and 68 (80% RH, I_{NaCl} = 5.1 mol kg^{-1}, $I_{(NH4)2SO4}$ = 17.5 mol kg^{-1}), i.e. this would lead to an enhancement effect in the kinetics. By contrast, calculations comparing $NaNO_3$ and NaCl media yield values similar to each other which is consistent with our experimental results. We neglected the activity coefficient of H_2SO_3 in these calculations, on the assumption that its variation across the different salt media would be much smaller than that of the product of the H^+ and HSO_3^- activity coefficients. Note that we cannot estimate what the ionic strength effects are for the rate constant in Equation (1) for sulfate solutions.

3 General acid catalysis

Fig. S6 shows that the measured sulfate formation rate increases with the increase of malonic acid concentration at relatively constant pH and ionic strengths (Exp# 13-18), providing clear evidence that malonic acid buffer catalyzes the aqueous oxidation of SO_2 by H_2O_2. The reaction rate coefficient of general acid catalysis k_{HX} has been found to be negatively correlated with the pKa* of acid (8) (Fig. S7B). Based on this relationship, $k_{malonic\ acid}$ is estimated to be 43 times higher than $k_{bimalonate}$, so the general acid catalysis induced by bimalonate can be neglected. The $k_{malonic\ acid}$ values for ionic strengths of 3.9 and 6.6 molal were then determined to be 5.61×10^5 and 1.32×10^5 $molal^{-2}$ s^{-1} from Fig. S6. We linearly fit these two rate constants (Fig. S7A) as a function of ionic strength. The ionic strength-dependent general acid catalyzed sulfate formation rate was then calculated (using Equation 1 in the main text) and subtracted from the measured sulfate formation rate to determine the proton-catalyzed sulfate formation rate. The justification for decreasing values for $k_{malonic\ acid}$ as a function of ionic strength is that the pKa* of malonic acid

195 increases with ionic strength for concentrated solutions (Fig. S7C). Fig. S7B demonstrates
196 that larger values of the pKa* lead to smaller values of $k_{malonic\ acid}$.

197 4 TMI experiments

198 We also utilized the kinetics flow tube to investigate the effects of ionic strength on
199 aqueous phase TMI catalyzed oxidation of dissolved SO_2 by O_2 in aerosol particles. The
200 experimental conditions are shown in Table S5. The pH-buffered polydisperse deliquesced
201 aerosol particles with three different concentrations of TMI were prepared by atomizing
202 the following solutions: a mixture of NaCl/malonic acid/sodium bimalonate (10/0.5/0.5
203 mM) with 1 μM iron (III) chloride ($FeCl_3$) and 50 μM, 0.2 mM, and 2 mM manganese (II)
204 chloride ($MnCl_2$), respectively. All experiments were conducted at pH of 2.8 to ensure high
205 solubility of Fe (III). Unlike the H_2O_2 experiments, the SO_2 flow for TMI experiments was
206 introduced into the central portion of the humidified aerosol flow through the movable
207 stainless steel tube, enabling variable reaction time. For an experimental run, the aerosol
208 particles were first characterized in the absence of SO_2 to quantify the background sulfate
209 in the seed aerosols. Then the aqueous oxidation of SO_2 was initiated by introducing SO_2.
210 The TMI experiments were conducted in air as a carrier gas, given that O_2 is the oxidant.

211 Modeled sulfate formation rates were calculated based on the literature parameters of
212 aqueous SO_2 oxidation by TMI+O_2 obtained in bulk solutions, without taking the effects
213 of ionic strength into account. The relevant rate expressions, rate coefficients and
214 equilibrium constants that we used to calculate the aqueous-phase concentrations of SO_2
215 are shown in Tables S2 and S3, respectively. Regarding the calculation of Fe (III) and Mn
216 (II) concentrations in the aerosol particles, the molality of NaCl in the aerosol particles was
217 first estimated using the E-AIM model (9). The Fe (III) and Mn (II) aerosols were expected

to undergo the same degree of concentration after atomization. The molality of Fe (III) and Mn (II) was then estimated from the NaCl molality accordingly. The Fe (III) concentration may be limited by the solubility of $Fe(OH)_3$ in which case the saturated concentration of Fe (III) was estimated from the solubility product equilibrium constant of Fe $(OH)_3$ (K_{sp} = 2.6×10^{-38}) (10). Table S5 shows a comparison between the measured and modeled sulfate formation rates for the TMI experiments. We find that the sulfate formation rate for TMI oxidation decreases by a factor of approximately 85 at an ionic strength of 2.8 molal compared to that calculated for the dilute solution. The effect of ionic strength can be well described by the extended Debye-Hückel equation (Fig. S8) (11, 12). The fitting parameter of -3.02 is within the range of -2 for Fe (III) and -4 for Mn (II) (11, 12). In the main paper Fig. 3, we note that we likely overestimate the sulfate formation rate that will prevail for the TMI oxidation pathway at high ionic strength by using the inhibition factor obtained at a lower ionic strength of 2.8 molal.

5 Uncertainties of aerosol pH and aerosol liquid water volume

Fig. S9 shows a comparison of aerosol pH for the mixture of NaCl and organic buffer estimated using the E-AIM and Pitzer models. The Pitzer model gave approximately 0.4 unit lower pH values for the mixture of NaCl/malonic acid/sodium bimalonate and 1 unit higher pH values for the mixture of NaCl/sodium bimalonate/sodium malonate compared to the E-AIM model results. The enhancement factors for the proton-catalyzed sulfate formation rate at the highest ionic strength (~14 molal) remain unchanged when the E-AIM aerosol pH was used for the calculation (Fig. S10A). Therefore, the aerosol pH differences between the E-AIM and Pitzer models will not impact our conclusions.

We also determined the aerosol liquid water volume by multiplying the total measured aerosol volume by the ratio of the aerosol liquid water volume to the total aerosol volume estimated using the E-AIM model. The estimated aerosol liquid water volume is 1.0–1.9, 3.2–3.4, 2.9–4.9, and 1.7–2.0 times higher than the measured aerosol liquid water volume for the mixture of NaCl and organic buffer, $NaNO_3$ and organic buffer, organic buffer at pH 2.8, and organic buffer at pH 3.9, respectively. Consequently, the enhancement factor for the proton-catalyzed sulfate formation rate at ionic strengths of 14 molal decreases to $19 \pm 3 – 30 \pm 5$ (Fig. S10B). The sulfate formation rate for the H_2O_2 reaction pathway in the main paper Fig. 3 will be lowered to 13.5–21.3 μg m^{-3} h^{-1}, remaining larger than the sulfate formation rates from other pathways. Therefore, using the estimated aerosol liquid water volume in the calculation will not impact our conclusion that the oxidation of SO_2 by H_2O_2 in aerosol particles can contribute to the missing sulfate source during severe haze episodes.

6 References

1. M. R. Canagaratna *et al.*, Chemical and microphysical characterization of ambient aerosols with the aerodyne aerosol mass spectrometer. *Mass Spectrom. Rev.* **26**, 185-222 (2007).
2. Y. Chen *et al.*, Response of the Aerodyne Aerosol Mass Spectrometer to Inorganic Sulfates and Organosulfur Compounds: Applications in Field and Laboratory Measurements. *Environ. Sci. Technol.* **53**, 5176-5186 (2019).
3. B. M. Matthew, A. M. Middlebrook, T. B. Onasch, Collection Efficiencies in an Aerodyne Aerosol Mass Spectrometer as a Function of Particle Phase for Laboratory Generated Aerosols. *Aerosol Sci. Technol.* **42**, 884-898 (2008).
4. I. N. Tang, H. R. Munkelwitz, Composition and temperature dependence of the deliquescence properties of hygroscopic aerosols. *Atmos. Environ.* **27**, 467-473 (1993).
5. F. J. Millero, J. B. Hershey, G. Johnson, J.-Z. Zhang, The solubility of SO2 and the dissociation of H2SO3 in NaCl solutions. *J. Atmos. Chem.* **8**, 377-389 (1989).
6. F. Maaß, H. Elias, K. J. Wannowius, Kinetics of the oxidation of hydrogen sulfite by hydrogen peroxide in aqueous solution:: ionic strength effects and temperature dependence. *Atmos. Environ.* **33**, 4413-4419 (1999).
7. H. M. Ali, M. Iedema, X. Y. Yu, J. P. Cowin, Ionic strength dependence of the oxidation of SO2 by H2O2 in sodium chloride particles. *Atmos. Environ.* **89**, 731-738 (2014).
8. C. Drexler, H. Elias, B. Fecher, K. J. Wannowius, Kinetic investigation of sulfur(IV) oxidation by peroxo compounds R-OOH in aqueous solution. *Fresenius J. Anal. Chem.* **340**, 605-615 (1991).
9. A. S. Wexler, S. L. Clegg, Atmospheric aerosol models for systems including the ions H+, NH4+, Na+, SO42−, NO3−, Cl−, Br−, and H2O. *J. Geophys. Res.-Atmos.* **107**, ACH 14-11-ACH 14-14 (2002).
10. T. E. Graedel, C. J. Weschler, Chemistry within aqueous atmospheric aerosols and raindrops. *Rev. Geophys.* **19**, 505-539 (1981).
11. L. Robbin Martin, M. W. Hill, The effect of ionic strength on the manganese catalyzed oxidation of sulfur(IV). *Atmos. Environ.* **21**, 2267-2270 (1987).
12. L. R. Martin, M. W. Hill, The iron catalyzed oxidation of sulfur: Reconciliation of the literature rates. *Atmos. Environ.* **21**, 1487-1490 (1987).
13. M. R. Hoffmann, J. G. Calvert, Chemical Transformation Modules for Eulerian Acid Deposition Models: Volume II, the Aqueous-phase Chemistry. *EPA/600/3-85* **17** (1985).
14. T. Ibusuki, K. Takeuchi, Sulfur dioxide oxidation by oxygen catalyzed by mixtures of manganese(II) and iron(III) in aqueous solutions at environmental reaction conditions. *Atmos. Environ.* **21**, 1555-1560 (1987).
15. J. H. Seinfeld, S. N. Pandis, *Atmospheric chemistry and physics: from air pollution to climate change* (John Wiley & Sons, 2016).
16. R. M. Kettler, D. J. Wesolowski, D. A. Palmer, Dissociation quotients of malonic acid in aqueous sodium chloride media to 100°C. *J. Solution Chem.* **21**, 883-900 (1992).

Table S1. SO_2/H_2O_2 experimental conditions and results.

Exp #	Aerosol type [a]	RH (%)	T (ºC)	SO_2 (ppb)	H_2O_2 (ppb)	Aerosol pH [b]	Ionic strength (molal)	Malonic acid (molal)	Bimalonate (molal)	Measured SO_4^{2-} formation rate (molal s^{-1})	Modeled SO_4^{2-} formation rate (molal s^{-1})[c]	Calculated proton-catalyzed SO_4^{2-} formation rate (molal s^{-1})[d]
1	A1	74	23	341	94	2.3	6.5	0.547	0.368	0.0112	0.0047	0.0033
2	A1	75	23	347	94	2.3	6.2	0.330	0.224	0.0107	0.0046	
3	B1	78	21	348	94	4.8	6.3	0.027	0.207	0.0129	0.0055	
4	B1	83	22	343	94	4.8	5.1	0.017	0.176	0.0149	0.0051	
5	B1	82	22	343	94	4.8	5.1	0.017	0.176	0.0124	0.0048	
6	B1	86	22	343	94	4.8	4.5	0.013	0.159	0.0101	0.0048	
7	A1	86	22	328	94	2.4	3.8	0.190	0.155	0.0125	0.0046	0.0072
8	A1	90	22	60	94	2.5	2.8	0.137	0.121	0.0021	0.0008	0.0015
9	A1	89	22	155	94	2.5	2.8	0.137	0.121	0.0047	0.0022	0.0029
10	A1	88	22	340	5	2.5	3.3	0.164	0.139	0.00031	0.00027	0.00005
11	A1	87	22	340	544	2.5	3.5	0.177	0.147	0.0730	0.0271	0.0463
12	A1	87	22	340	94	2.5	3.5	0.177	0.147	0.0100	0.0047	0.0054
13	A1	74	23	345	94	2.3	6.5	0.547	0.368	0.0197	0.0044	0.0124
14	A2	73	24	345	94	2.3	6.7	1.060	0.705	0.0272	0.0043	0.0171
15	A3	73	24	345	94	2.3	6.8	2.452	1.664	0.0409	0.0043	0.0217
16	A1	85	25	316	94	2.4	4.0	0.203	0.163	0.0103	0.0036	0.0066
17	A2	85	24	316	94	2.4	3.9	0.595	0.480	0.0156	0.0036	0.0044
18	A3	85	25	316	94	2.4	3.8	1.326	1.083	0.0306	0.0036	0.0055
19	B1	79	24	350	94	4.8	5.9	0.024	0.198	0.0146	0.0044	
20	B2	78	24	350	94	4.8	7.3	0.068	0.584	0.0246	0.0041	
21	B3	78	24	350	94	4.8	8.8	0.121	1.207	0.0427	0.0041	0.0427
22	C	78	23	245	221	2.8	8.5	0.431	0.354	0.0616	0.0074	0.0616
23	D	78	23	245	221	4.0	9.4	0.024	0.343	0.0714	0.0075	0.0714
24	E	73	22	359	94	2.8	7.1	7.055	5.251	0.0683	0.0050	
25	F	74	22	359	94	3.9	14.5	0.256	3.043	0.1644	0.0050	0.1644
26	E	75	21	70	94	2.8	6.4	6.381	4.847	0.0225	0.0011	
27	E	75	21	179	94	2.8	6.4	6.381	4.847	0.0329	0.0028	
28	F	74	21	179	94	3.9	14.5	0.256	3.043	0.1426	0.0028	0.1426
29	E	75	23	349	94	2.8	6.4	6.381	4.847	0.0558	0.0047	
30	F	75	23	349	94	3.9	14.0	0.244	2.947	0.1958	0.0048	0.1958

[a] Six types of seed aerosols. A: NaCl/malonic acid/sodium bimalonate (A1: molar ratio of 20:1:1; A2: molar ratio of 6:1:1; A3: molar ratio of 2:1:1); B: NaCl/sodium bimalonate/sodium malonate (B1: molar ratio of 20:1:1; B2: molar ratio of 6:1:1; B3: molar ratio of 2:1:1); C: $NaNO_3$/malonic acid/sodium bimalonate (molar ratio of 20:1:1); D: $NaNO_3$/sodium bimalonate/sodium malonate (molar ratio of 20:1:1); E: malonic acid/sodium bimalonate (molar ratio of 1:1); F: sodium bimalonate/sodium malonate (molar ratio of 1:1).

[b] Aerosol pH of type A and B was estimated using the Pitzer model; C, D, E and F was estimated using the E-AIM model.

[c] Modeled sulfate formation rates were calculated based on the literature parameters of aqueous SO_2 oxidation by H_2O_2 obtained in bulk solutions, without taking the effects of ionic strength and general acid catalysis into account.

[d] The calculated proton-catalyzed sulfate formation rates were determined by subtracting the general acid catalyzed sulfate formation rate from the measured sulfate formation rate. For experiments 2-6, 19, 20, 24, 26, 27, and 29, the measured sulfate formation rates were lower than the estimated general acid catalysis sulfate formation rates; therefore, the calculated proton-catalyzed sulfate formation rates for these experiments were negative and not presented.

311 **Table S2. Aqueous reactions rate expressions and rate coefficients.**

Oxidants	Sulfate formation rate (molal s^{-1})	Reference
H_2O_2	$k'[H^+][HSO_3^-][H_2O_2(aq)]/(1+K[H^+])$ $k' = 7.45\times10^7\times e^{(-4430\times(1/T-1/298))}$ M^{-2} s^{-1} $K = 13$ M^{-1}	Hoffmann and Calvert (13)
TMI+O_2	$k_2[H^+]^{-0.74}[S(IV)][Mn(II)][Fe(III)]$ (pH ≤ 4.2) $k_2 = 3.72\times10^7$ M^{-2} s^{-1} $k_3[H^+]^{0.67}[S(IV)][Mn(II)][Fe(III)]$ (pH > 4.2) $k_3 = 2.51\times10^{13}$ M^{-2} s^{-1}	Ibusuki and Takeuchi (14)

312

Table S3. Equilibrium constants for calculating aqueous-phase concentrations.

Species	Aqueous-phase concentration expressions	Equilibrium constants[a]	References
SO_2	$[H_2SO_3]=H_{SO_2}\times p_{SO_2}$	$H_{SO_2}=1.23\times e^{(3145.3\times(\frac{1}{T}-\frac{1}{298}))}$	Seinfeld and Pandis (15)
	$[HSO_3^-]=K_{a1}\times[H_2SO_3]/[H^+]$	$K_{a1}=1.3\times10^{-2}\times e^{(1960\times((\frac{1}{T}-\frac{1}{298}))}$	
	$[SO_3^{2-}]=K_{a2}\times[HSO_3^-]/[H^+]$	$K_{a2}=6.6\times10^{-8}\times e^{(1500\times((\frac{1}{T}-\frac{1}{298}))}$	
H_2O_2	$[H_2O_2(aq)]=H_{H_2O_2}\times p_{H_2O_2}$	$H_{H_2O_2}=1.3\times10^{5}\times e^{(7297.1\times(\frac{1}{T}-\frac{1}{298}))}$	Seinfeld and Pandis (15)

[a] H and K_a are in units of M atm^{-1} and M, respectively.

315 **Table S4. Ionic strength (*I*) effects on aqueous reaction rate coefficient and**
316 **equilibrium constants.**

Parameter	Expressions	Notes	References
	$\frac{dSO_4^{2-}}{dt} = (k + k_{HX}[HX][H^+]^{-1})K_{a1}^* H_{SO_2} P_{SO_2} H_{H_2O_2} P_{H_2O_2}$		
k	$\log\left(\frac{k}{k^{I=0}}\right) = 0.36I - \frac{1.018\sqrt{I}}{1+0.17\sqrt{I}}$	I_{max} = 5 molal	Maaβ et al. (6)
$H_{H_2O_2}$	$\frac{H_{H_2O_2}}{H_{H_2O_2}^{I=0}} = 1 - 1.414\times10^{-3} I^2 + 0.121I$	I_{max} = 5 molal	Ali et al. (7)
H_{SO_2}	$\log\left(\frac{H_{SO_2}}{H_{SO_2}^{I=0}}\right) = \left(\frac{22.3}{T} - 0.0997\right)\times I$	I_{max} = 6 molal	Millero et al. (5)
K_{a1}^*	$\log\left(\frac{K_{a1}^*}{K_{a1}^{I=0}}\right) = 0.5\times\sqrt{I} - 0.31\times I$	I_{max} = 6 molal	Millero et al. (5)
K_{a2}^*	$\log\left(\frac{K_{a2}^*}{K_{a2}^{I=0}}\right) = 1.052\times\sqrt{I} - 0.36\times I$	I_{max} = 6 molal	Millero et al. (5)

317

Table S5. SO_2/TMI experimental conditions and results.

Exp #	Aerosol type [a]	RH (%)	T (ºC)	SO_2 (ppb)	Aerosol pH	Fe (III) (mmolal) [b]	Mn (II) (mmolal) [b]	Ionic strength (molal)	Measured SO_4^{2-} formation rate (molal s^{-1})	Modeled SO_4^{2-} formation rate (molal s^{-1})
31	G	92	22	316	2.8	0.194 [c]	11.5	2.34	0.000621	0.046
32	H	94	22	307	2.8	0.176	352	2.82	0.015	1.277
33	I	94	24	292	2.8	0.176	35.2	1.87	0.0024	0.109

[a] Three types of seed aerosols. G: NaCl/malonic acid/sodium bimalonate/$FeCl_3$/$MnCl_2$ (10/0.5/0.5/0.001/0.05 mM) in atomizer solution; H: NaCl/malonic acid/sodium bimalonate/$FeCl_3$/$MnCl_2$ (10/0.5/0.5/0.001/2 mM) in atomizer solution; I: NaCl/malonic acid/sodium bimalonate/$FeCl_3$/$MnCl_2$ (10/0.5/0.5/0.001/0.2 mM) in atomizer solution.

[b] For each experiment, the molality of NaCl in the aerosol particles was first estimated using E-AIM model (9). The Fe (III) and Mn (II) aerosols were expected to undergo the same degree of concentration after atomization. The molality of Fe (III) and Mn (II) was then estimated from the NaCl molality accordingly.

[c] The Fe (III) concentration may be limited by the solubility of $Fe(OH)_3$ for Exp # 31. The saturated concentration of Fe (III) was estimated from the precipitation equilibrium of $Fe(OH)_3$ ($K_{sp} = 2.6\times 10^{-38}$) (10).

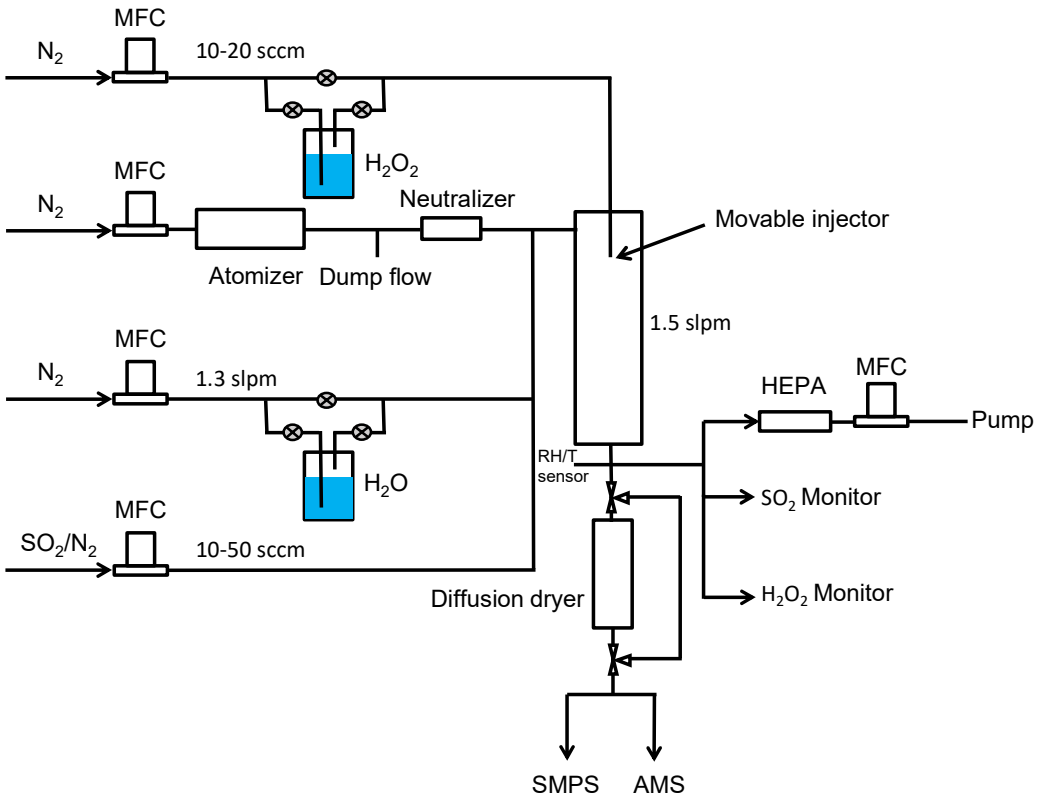

329

330 **Fig. S1.** Schematic of the experimental setup.

331

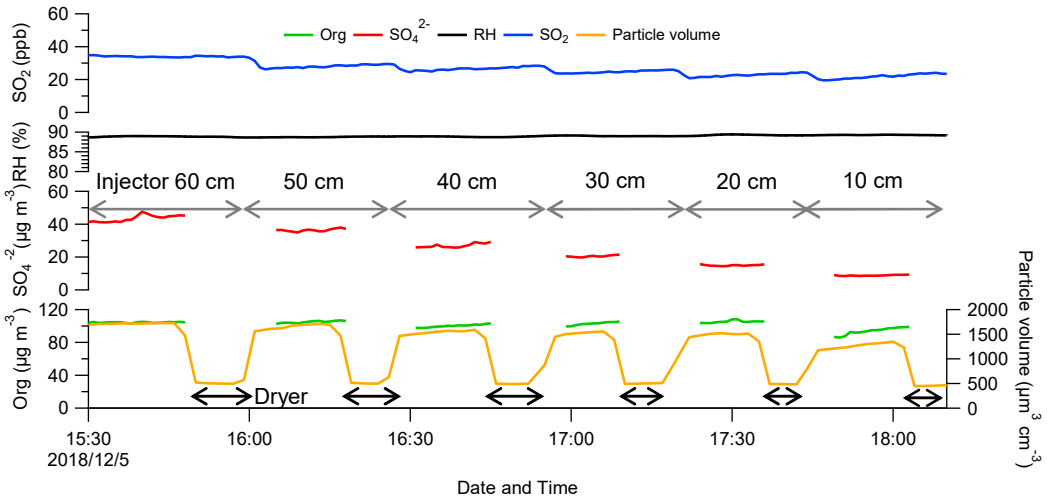

Fig. S2. Time series of RH, SO_2, particle volume, organics and sulfate concentrations for an experiment during which the aerosol water content was measured at each position, showing that it remains stable. For most experiments, the AWC was only measured once during the experiment.

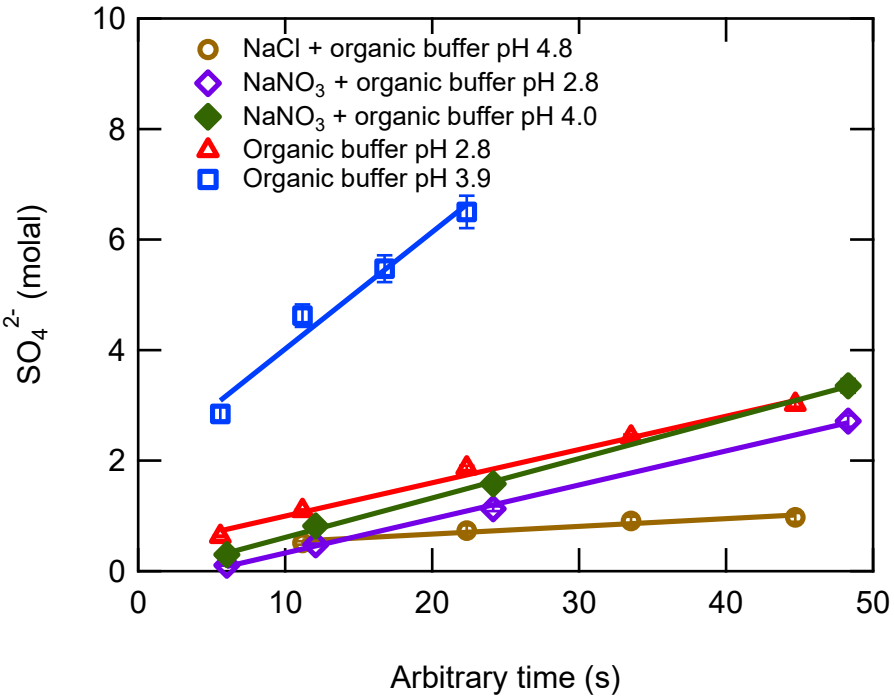

338

339 **Fig. S3.** Kinetics of aqueous oxidation of SO_2 by H_2O_2 in a mixture of NaCl and malonic

340 acid buffer aerosol particles at pH 4.8 (Exp# 3), $NaNO_3$ and malonic acid buffer aerosol

341 particles at pH 2.8 (Exp# 22) and pH 4.0 (Exp# 23), malonic acid buffer aerosol particles

342 at pH 2.8 (Exp# 29) and 3.9 (Exp# 30).

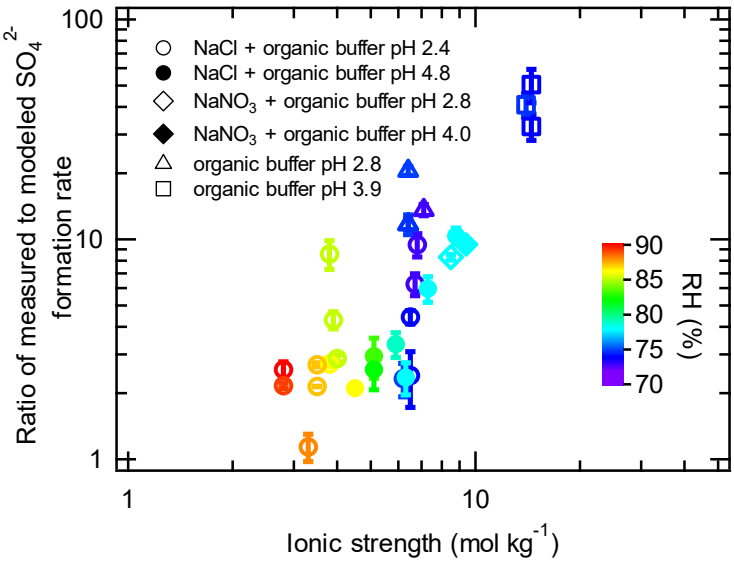

343

344 **Fig. S4.** Dependence of the ratio of the measured to modeled sulfate formation rate on

345 ionic strength and RH.

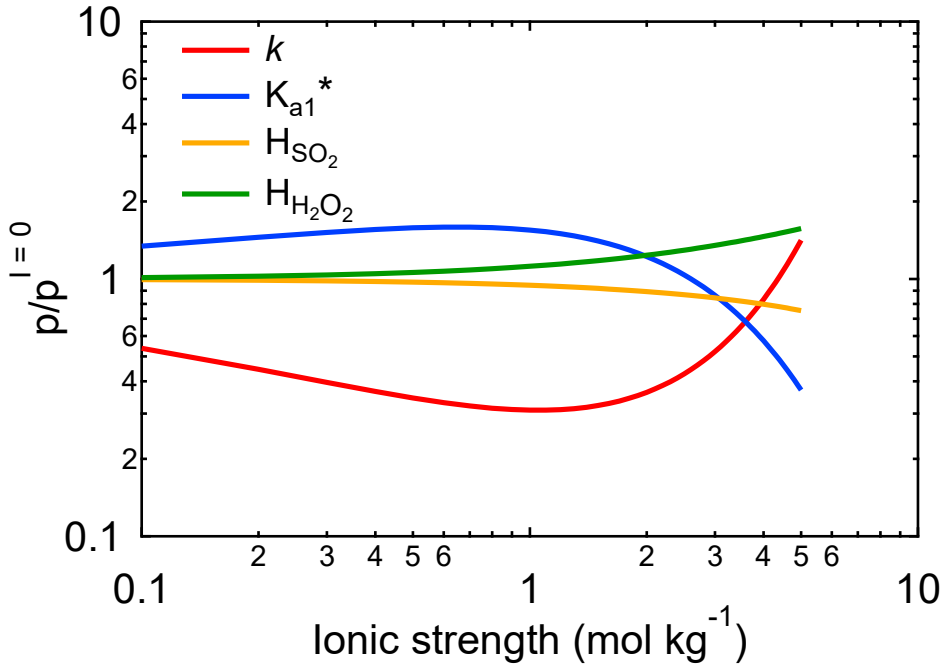

346

347 **Fig. S5.** Effects of ionic strength on aqueous reaction rate coefficient and stoichiometric

348 equilibrium constants for the SO_2-H_2O_2 reaction. The parameter p represents the reaction

349 rate coefficient or equilibrium constants.

350

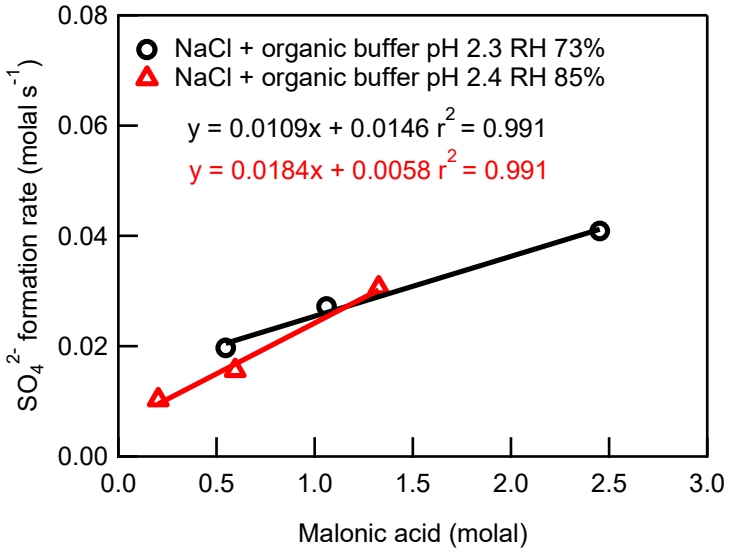

351

352 **Fig. S6.** Plot of sulfate formation rate as a function of malonic acid concentration for a

353 mixture of NaCl and malonic acid buffer aerosol particles at pH 2.3 at RH of 73% (I =

354 6.6 molal, Exp# 13-15) and pH 2.4 at RH of 85% (I = 3.9 molal, Exp# 16-18).

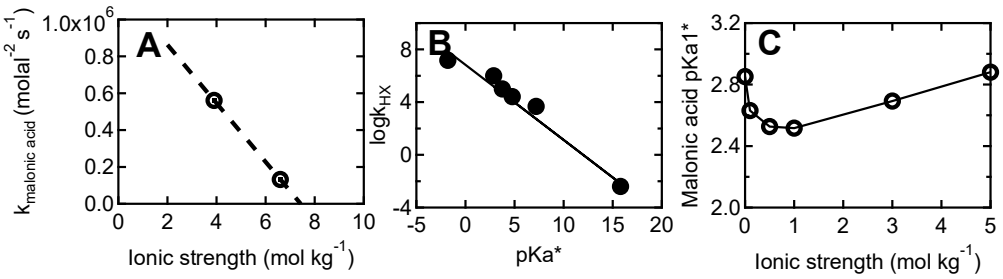

355

356 **Fig. S7 (A)** Dependence of $k_{malonic\ acid}$ on the ionic strength. The $k_{malonic\ acid}$ data for ion
357 strengths of 3.9 and 6.6 molal were determined from Fig. S6, using Equation (1) and the
358 calculated molality of H^+. The fitting equation is $k_{malonic\ acid} = -1.59\times10^5 I + 1.18\times10^6$ **(B)** Plot
359 of log k_{HX} versus pKa* of acid HX at 285 K and ionic strength of 0.5 molal. This figure is
360 adapted from Drexler et al. (8) and the units for k_{HX} are $M^{-2}\ s^{-1}$. The fitting equation is log
361 $k_{HX} = -0.57$pKa* (HX) + 6.83. **(C)** Dependence of the first pKa* of malonic acid on the
362 ionic strength. This figure is adapted from Kettler et al. (16).

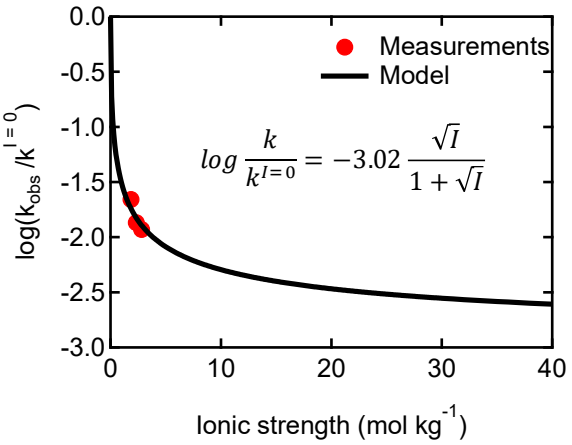

363

364 **Fig. S8** Impact of ionic strength on the sulfate formation rate of aqueous phase TMI-
365 catalyzed oxidation of dissolved SO_2 by O_2 in aerosol particles. The effect of ionic strength
366 can be well described by the extended Debye-Hückel equation (11, 12), shown as an inset
367 in the figure. The fitting parameter of -3.02 is within the range of -2 for Fe (III) and -4 for
368 Mn (II) (11, 12).

369

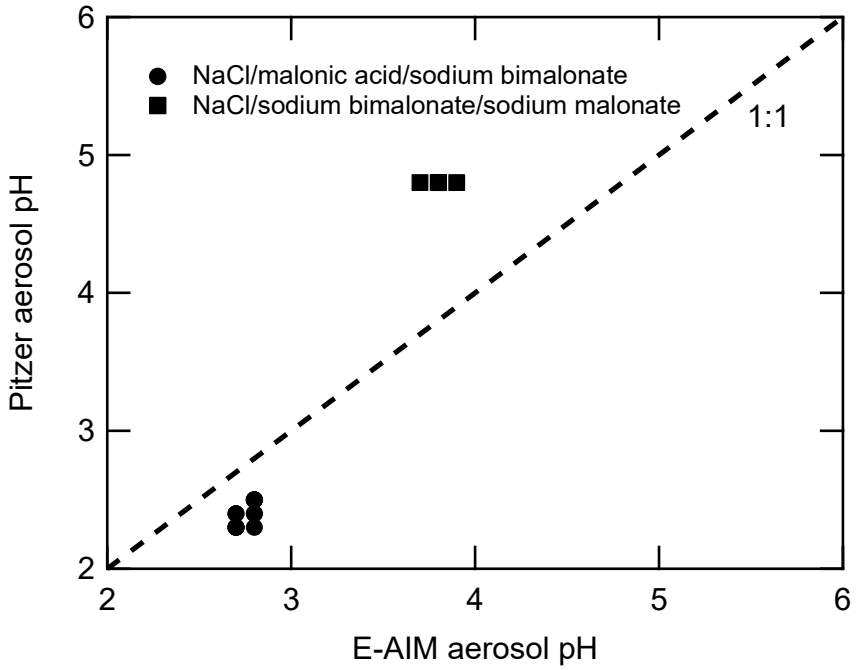

370

371 **Fig. S9** Comparison of aerosol pH for the mixture of NaCl and organic buffer calculated

372 using the Pitzer and E-AIM models.

373

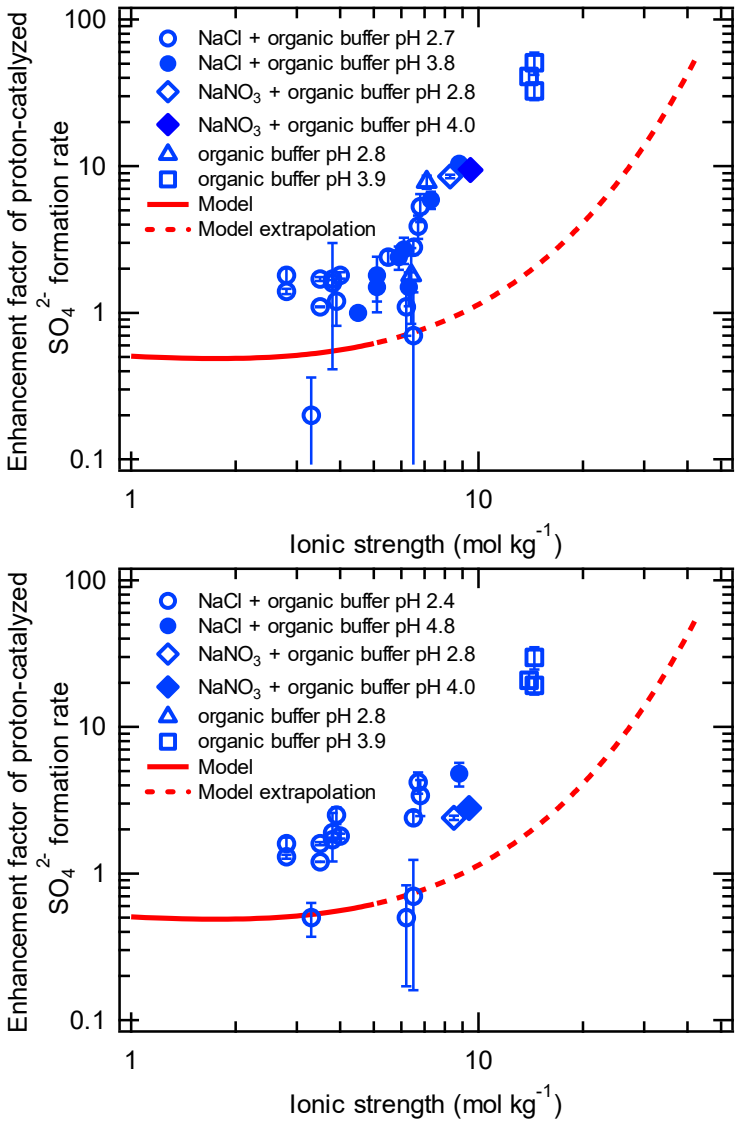

374

375 **Fig. S10** Dependence of the enhancement factor of proton-catalyzed sulfate formation rate
376 on ionic strength. **(A)** Aerosol pH for the mixture of NaCl and organic acid buffer was
377 estimated using the E-AIM model. **(B)** Aerosol liquid water volume was determined by
378 multiplying the total measured aerosol volume by the ratio of the aerosol liquid water
379 volume to the total aerosol volume estimated using the E-AIM model.